

## RESEARCH ARTICLE

# Anomaly Detection Method of BDS Signal-in-Space Based on Autoregressive Distributed Lag Model

LIANG LIU<sup>1</sup>, HUICHAO LIU<sup>2</sup>, ERSHEN WANG<sup>1,2</sup>, TENGLI YU<sup>1,3</sup>, SHIYU JIA<sup>1</sup>, TENG LONG<sup>1</sup>, AND XINHUI SUN<sup>2</sup>

<sup>1</sup>54th Research Institute of China Electronics Technology Group Corporation, Shijiazhuang 050001, China

<sup>2</sup>School of Electronic and Information Engineering, Shenyang Aerospace University, Shenyang 110136, China

<sup>3</sup>School of Aerospace Engineering, Shenyang Aerospace University, Shenyang 110136, China

Corresponding author: Ershen Wang (wes2016@sau.edu.cn)


This work was supported in part by the National Natural Science Foundation of China under Grant 62173237; in part by the Open Fund of State Key Laboratory of Satellite Navigation System and Equipment Technology under Grant CEPNT2022B04; in part by the SongShan Laboratory Foundation under Grant YYJC062022017; in part by the Open Fund of Key Laboratory of Civil Aviation Flights Wide Area Surveillance and Safety Control Technology, Civil Aviation University of China, under Grant 202105; in part by the Applied Basic Research Programs of Liaoning Province under Grant 2022020502-JH2/1013; in part by the Open Fund of Key Laboratory of Flight Techniques and Flight Safety Civil Aviation Administration of China (CAAC) under Grant FZ2021KF15 and Grant FZ2021ZZ06; in part by the Special Funds Program of Civil Aircraft under Grant 01020220627066; and in part by the Special Funds Program of Shenyang Science and Technology under Grant 22-322-3-34.

**ABSTRACT** The signal-in-space (SIS) anomaly of BeiDou navigation satellite system (BDS) is an important factor affecting its high accuracy SIS quality assessment. Detecting and eliminating SIS anomaly is not only an important method to build SIS fault model of BDS, but also helps to guarantee the integrity of BDS navigation and positioning. Based on the problem that the traditional empirical threshold method cannot accurately identify the start and end times of anomalies in anomaly detection, which leads to anomaly detection leakage, a combined detection method based on autoregressive distributed lag model and empirical threshold is proposed in this paper. Before the calculation, the spurious anomalies of SIS are removed by data cleaning. The high-precision SIS ranging error (SISRE) is recovered by Space State Representation (SSR) correction number, and then projected to the user's line of sight direction, and the anomaly detection threshold is determined by using the combined threshold of empirical threshold and autoregressive distributed lag (ARDL) model. The feasibility and effectiveness of the method were analyzed by using the data collected in 2021. The test results show that compared with the traditional threshold method, the proposed method can more accurately detect the start and end points of SIS anomalies caused by clock anomalies, thereby improving the detection accuracy. In addition, the anomaly detection method proposed in this paper is used to count the anomalies throughout the year, and the results show that the highest frequency of anomalies is found in geostationary orbit (GEO) and inclined geosynchronous orbit (IGSO), and these anomalies are mainly caused by satellite clocks.

**INDEX TERMS** BeiDou navigation satellite system (BDS), signal-in-space (SIS), signal-in-space anomaly, clock anomaly.

## I. INTRODUCTION

The broadcast ephemeris is essential for real-time navigation and positioning, as it allows satellites to be affected by SIS

The associate editor coordinating the review of this manuscript and approving it for publication was Jing Liang .

performance - such as clock stability, predictability of orbital maneuvers, and control terminal performance, including orbit and clock resolution performance, distribution of monitoring stations, and injection capabilities [7]. However, satellite orbit and clock data broadcasted by the navigation ephemeris are sometimes biased. The deviation between the broadcasted

orbits and clocks and their true values is uniformly referred to as SIS error, which is referred to in this paper as broadcast ephemeris SIS error. However, the broadcast ephemeris SIS error is so large that it does not meet the needs of users. In order to meet the navigation and positioning needs of the majority of real-time users, the International GNSS Service (IGS) officially launched the real-time pilot project (RTPP) in June 2007 and officially provided real-time precision products in April 2013. The server side provides a number of corrections based on state space representation (SSR), such as satellite clock difference correction, satellite orbit correction, satellite signal deviation, etc. The state space of satellite navigation and positioning is composed of these errors together, providing high precision SIS corrections [2]. In general, assuming that the broadcast ephemeris, real-time orbit, and real time clock error corrections are reliable, the broadcast ephemeris SISRE is in the meter to submeter range, and the high precision SISRE corrected by the corrections can be improved to the centimeter to submeter rang [3]. However, SIS exceptions can occasionally occur, either due to abnormal operation of the onboard device or incorrect ephemeris uploaded by Constellation service providers (CSP) [4].

The SIS URE is projected by the SISRE in the direction of the users' line of sight and represents the effect of satellite orbit and clock errors on the user's observations, which is also an effective component affecting the positioning accuracy [5]. In order to characterize SIS URE, user range accuracy (URA) provides a conservative estimate of SIS URE without anomalous effects, so it is necessary to distinguish between normal SIS URE and anomalous SIS URE. For the above two types of SIS URE, there are two main research methods for post-analysis and real-time estimation. The post-analysis method uses the satellite orbits and clock products provided by the ex-post precision ephemeris as a baseline to calculate the broadcast ephemeris SIS URE. Real-time SIS URE estimation is based on ground-based stations, using pseudo-range observations, to estimate the SIS URE on the satellite terminal [6].

Scientists around the world have been exploring the SIS anomaly for a long time. Heng et al. studied GPS SIS anomalies from 2000 to 2010 by comparing broadcast ephemeris and precision ephemeris and showed that about 10% of the anomalies resulted in a worst-case SIS URE greater than 10 times the upper bound (UB) of the URA, and about 1% of the anomalies resulted in a worst-case SIS URE greater than 100 times the URA UB [7]. Wu et al. conducted a preliminary analysis of SIS anomalies in BDS using precision ephemeris data from 2013 to 2015, but did not fully consider subtracting constellation anomalies caused by satellite clock anomalies from the clock data and did not systematically analyze the types and effects of the anomalies [8]. Walter et al. analyzed historical data of GLONASS from 2009 to 2016 and found that the satellite failure rate decreased to below  $10^{-4}$  over the eight-year period studied, but the constellation failure rate did not meet the corresponding commitment [9]. To address the issue of real-time detection, Tu et al. developed a method for

computing instantaneous URE (IURE) and derived an empirical threshold through statistical analysis of IURE prior to detecting SIS anomalies. This approach successfully resolves the limitations of the conventional method of comparing broadcast and post-processed precise ephemeris. The results indicated that SIS anomalies caused by clock jumps were predominant and could exceed tens of thousands of meters in magnitude, but the proposed method accurately identified their starting and ending times. Nonetheless, it is noteworthy that while the ending time remained precise, the starting time was slightly delayed compared to the actual occurrence time [10]. An improved SIS anomaly detection method based on accurate ephemeris was proposed by Tu et al. [10] and the results showed that the method can greatly reduce the occurrence of constellation faults caused by satellite clock errors compared to the traditional empirical threshold method [11]. C Ouyang. et al. conducted anomaly detection of SIS from 2013 to 2018 using both broadcast and precise ephemeris, with the aim of studying the long-term abnormal behavior of space signals. The results indicated that URAI was incapable of reflecting any anomalies in satellites. And a total of 20,241 abnormal messages were detected. In these abnormal navigation messages, 18,432 were recognized as orbit anomalies, which is much more frequent than the 2011 clock anomalies [12]. With the aim of assessing the abnormal conditions of the Galileo constellation, L. Fan. et al. conducted anomaly detection on all healthy Galileo satellites from 2017 to 2018 using precise ephemeris, and obtained detection thresholds by statistical analysis of SIS errors. The findings revealed that the SIS anomalies in Galileo satellites were primarily caused by satellite clock errors, with magnitudes occasionally reaching several tens or even hundreds of meters [13].

The orbit and clock errors of satellites have strong time dependence, and their orbit and clock errors are affected by the previous moment errors, which are accompanied by regular changes when the satellite has space signal anomalies [14]. The relatively weak anomalous correlation error is ignored in the calculation of SISRE generated by broadcast ephemeris due to its poor accuracy. However, the errors affected by correlations cannot be ignored when calculating high-precision SISREs due to their high accuracy [14]. The above studies of spatial signal anomalies have not estimated the influence of time-dependent errors on the anomalies, which are called trending anomalies in this paper. To accurately identify SIS trending anomalies, an anomaly detection method based on the combination of the ARDL model and the empirical threshold is proposed in this paper. Data cleaning is first performed on the data source, thereby eliminating spatial signal pseudo-anomalies caused by receiver acceptance errors or data logging errors. The method is then used to determine the double anomaly detection threshold. The feasibility and effectiveness of the method are verified using ephemeris and real-time orbital clock correction data from 2021. The accumulated time of one-year anomalies of the satellite SIS of BDS was obtained. The results of this study

can provide valid a priori information for SIS system fault classification assessment and BDS availability and continuity performance assessment.

**II. DATA SOURCES AND PREPROCESSING STRATEGIES**

The determination of the number of independent samples is critical for error overbound. Inferring properties of the underlying error distribution from a given error dataset is always challenging. The data needs to be cleaned by us, in order to exclude the false anomalies of SISRE.

**A. DATA SOURCE**

The performance of BDS-2 and BDS-3 is evaluated for a period of 1 year from January 2021 to January 2022. IGS MGEX provides daily integrated broadcast ephemeris by merging observations from GNSS tracking stations, a product called BRDM, which shows satisfactory continuity during the analysis period and is therefore used as the main broadcast ephemeris data source in this study. Therefore, the RINEX V3 format broadcast ephemeris file generated by the MGEX analysis center was used in this study. The precision ephemeris contains accurate satellite orbit information and clock difference information and is of the same order of magnitude as the real satellite orbit parameters with an error of only a few centimeters, so it is considered that the precision ephemeris can replace the real satellite orbit elements in the calculation of SISRE. The precision ephemeris is generated by the IGS MGEX analysis center and is available from the public database. The CLK93 mount point of CNES (the name of the mount point was renamed to SSRA00CNE0 on January 6, 2021) is selected for real-time orbit and clock data and is used to receive the SSR data stream in real time through the BNC software.

**B. PREPROCESSING STRATEGY**

Since 135,000 navigation messages are corrupted by data recording errors every year, 11 false anomalies of the spatial signal correspond to one true anomaly [16]. Therefore, removing data logging errors from the raw data is an important pre-processing step before calculating SISRE.

In addition to the BDS-2 constellation, the real-time data stream CLK93 uploaded by CNES started to support the BDS-3 constellation in February 2020, and precision corrections for 18 BDS-3 MEO, 3 BDS-2 MEO, 7 BDS-2 IGSO and 5 BDS-2 GEO satellites can be provided by this data stream. Therefore, the data pre-processing section includes only the satellites supported by the CLK93/SSRA00CNE0 data stream.

Other data from the same time period that meet any of the above conditions will be excluded from this paper due to any type of error or missing data that would make it impossible to evaluate in this time period.

1. Not receiving real-time orbit and clock correction information.
2. The precision ephemeris/clock is missing or set to invalid values, such as “999, 999.9999” or “NAN”.
3. The broadcast ephemeris is not within the 4 h period.
4. The integrity status mark is not zero.
5. The navigation message is unhealthy, i.e. the health status mark is “1”.

**III. METHODOLOGY**

The orbit and clock errors of a satellite exhibit strong temporal correlations and are affected by errors from previous time steps. Regular changes often accompany spatial signal anomalies in satellites [4]. When calculating the SISRE produced by broadcast ephemeris, the relatively weak error correlation caused by anomalies is often ignored due to poor accuracy. However, when calculating high-precision SISRE, the errors influenced by correlation cannot be ignored due to their higher accuracy. None of the studies on spatial signal anomalies mentioned above have considered the impact of time-correlated errors on anomalies, which this paper refers to as trend anomalies. To more accurately identify SIS trend anomalies, this paper proposes a combined anomaly detection method based on the ARDL model and empirical thresholds, which can accurately identify the start time of trend faults and reduce the missed detection rate.

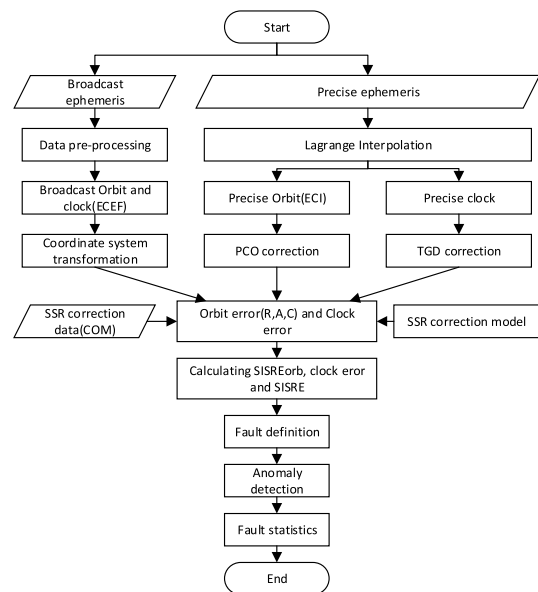


**FIGURE 1. Anomaly detection program of the BeiDou navigation satellite system.**

**A. HIGH PRECISION ORBIT AND CLOCK RECOVERY FOR BDS**

The satellite orbital position provided by the precision ephemeris is based on the center of mass (COM) of the satellite, while the broadcast ephemeris is based on the antenna phase center (APC) of the satellite. However, since the BDS broadcast track refers to the antenna reference point near the center of mass, the antenna offset correction is used [17].

Currently, the BDS real-time product from CNES (CLK93/SSRA00CNE0) has a sampling interval of 5 s. Therefore, theoretically, each satellite will receive 17,280

corrections per day. The real-time orbit correction message contains radial, along-track, and cross-track correction parameters, and the real-time user selects the corresponding satellite orbit parameters based on the data age in the SSR message [17]. The SSR orbit message gives the radial, along-track, and cross-track coordinate correction components in the satellite fixed coordinate system. The orbital correction number of the satellite at moment can be calculated by the following equation [19].

$$\delta O = \begin{bmatrix} \delta O_{radial} \\ \delta O_{along} \\ \delta O_{cross} \end{bmatrix} + \begin{bmatrix} \delta \dot{O}_{radial} \\ \delta \dot{O}_{along} \\ \delta \dot{O}_{cross} \end{bmatrix} (t - t_0) \quad (1)$$

where  $\delta O$  and  $\delta \dot{O}$  are the three directional correction components and velocity components at the reference moment  $t_0$ , which can be obtained in the SSR correction 1259 message type. The satellite correction position is calculated according to the following equation [20], [21].

$$X_{orbit} = X_{broadcast} - [e_{radial} \quad e_{along} \quad e_{cross}] \delta O \quad (2)$$

The SSR clock correction information contains the correction parameter  $\delta C$  used to correct the broadcast satellite clock. The polynomial representation describes the clock difference over a certain time period. The satellite clock difference correction information at time  $t$  can be calculated by the following equation.

$$\delta C = C_0 + C_1 (t - t_0) + C_2 (t - t_0)^2 \quad (3)$$

where  $t_0$  is the reference time obtained from the SSR orbit correction message;  $C_i$  is the polynomial coefficient from the SSR clock correction message. The precision satellite clock difference can be recovered by using the clock difference information calculated from the SSR message to correct the broadcast ephemeris satellite clock difference.

$$t_{satellite} = t_{broadcast} - \frac{\delta C}{c} \quad (4)$$

where,  $t_{broadcast}$  is the satellite time by the broadcast clock parameter, identified by the IODC of the corresponding SSR orbit correction information;  $t_{satellite}$  is the satellite time corrected by the SSR clock correction information;  $\delta C$  is the clock correction obtained from the SSR clock correction information;  $c$  is the speed of light.

## B. CALCULATION METHOD OF HIGH PRECISION SISRE

To generate high-precision orbit and clock residuals, the restored orbit and clock from Section III-A were compared with a posteriori precise ephemeris. The high-precision orbit and clock residuals were then utilized to further compute SISRE. SISRE is a source of error in the spatial segment during satellite signal transmission, which describes the statistical uncertainty in the spatial segment error caused by ephemeris errors [22]. SISRE, as one of the main error sources of pseudorange measurement, directly affects positioning accuracy and integrity. Therefore, the correct calculation of high-precision SISRE is a prerequisite for

anomaly detection and exclusion. In order to obtain the orbit and clock errors between broadcast ephemeris and precision ephemeris, one needs to convert their coordinates. The three components of the phase center deviation of the satellite antenna are in the star-fixed coordinate system, and the broadcasted orbit correction number is in the satellite orbit coordinate system, so the conversion between the star-fixed coordinate system, Earth-centered Earth-fixed, and geometric inertial coordinate systems is needed to correct the antenna phase center to the satellite mass center position, and finally the orbit-only SISRE and the SISRE [23].

For the calculation method of global average SISRE of BDS, the SISRE calculation models of the three orbits are different due to the different observation geometries of different orbits of BDS, and the calculation models are as follows [24].

$$\text{SISRE}_{\text{IGSO GEO}} = \sqrt{(0.99R - T)^2 + \frac{1}{127} (A^2 + C^2)} \quad (5)$$

$$\text{SISRE}_{\text{MEO}} = \sqrt{(0.98R - T)^2 + \frac{1}{54} (A^2 + C^2)} \quad (6)$$

where R represents the radial error, A represents the along-track error, and C represents the cross-track. R, A, and C are the three directions of the orbital error, respectively. T represents the clock error.

For the orbit-only SISRE, the pure orbital RMS SISRE is obtained by eliminating the clock error.

$$\text{SISRE}_{\text{OrbMEO}} = \sqrt{(0.98R)^2 + \frac{1}{54} (A^2 + C^2)} \quad (7)$$

$$\text{SISRE}_{\text{OrbIGSO/OrbGEO}} = \sqrt{(0.99R)^2 + \frac{1}{127} (A^2 + C^2)} \quad (8)$$

The International Terrestrial Reference Frame (ITRF) frame is used by the precision orbit products provided by IGS MGEX. The broadcast orbits of different systems are characterized under different coordinate systems, among which the satellite positions calculated by the broadcast ephemeris of the BDS system belong to CGCS2000. However, their differences of only a few centimeters to the scale are considered to be consistent [25], so their difference values can be ignored in this study. The BDS broadcast clock is referenced to a single-frequency B3I signal. However, the BDS precise clock released by MGEX is calculated by using the dual-frequency (B1I and B2I) ionospheric-free observations and is referenced to GPS Time (GPST). Therefore, even if the time bias of 14 seconds is eliminated, the time group delay (TGD) should be considered before the SSR DCB correction is introduced. Its TGD correction model is as follows [26].

$$\text{tgd}_{\text{brdc}}^i = \frac{f_{B1}^2}{f_{B1}^2 - f_{B2}^2} * \text{tgd}_1^i - \frac{f_{B2}^2}{f_{B1}^2 - f_{B2}^2} * \text{tgd}_2^i \quad (9)$$

where  $\text{tgd}_1^i$ ,  $\text{tgd}_2^i$  denote the time group delay corrections for PRN<sub>i</sub> in the B1I and B2I frequencies broadcast in the navigation ephemeris, respectively.  $\text{tgd}_{\text{brdc}}^i$  denotes the TGD

correction between the real clock difference of PRN<sub>i</sub> and the posterior precision clock difference.

$$dt^i = (t^i - \text{tgd}_{\text{brdc}}^i - T^i) \quad (10)$$

where  $dt^i$  is the difference between the dual-band TGD corrected real-time clock  $t^i$  and the ex-post precision clock  $T^i$ .

### C. AUTOREGRESSIVE DISTRIBUTION LAG MODEL

The previous section primarily discussed the computational model of SISRE. This chapter will further delve into the anomaly detection of SISRE. SIS anomalies are mainly caused by incorrect navigation data, orbital maneuvers, abnormal orbital perturbations, clock jumps, clock drift and other anomalous events [27]. Figure 2 shows the flow of a traditional threshold fault detection by simulating a slide fault. At the beginning of this fault, the SISRE value is below the threshold, but there is a clear trend of anomalies. The portion of the fault below the threshold is not detected by the conventional threshold method.

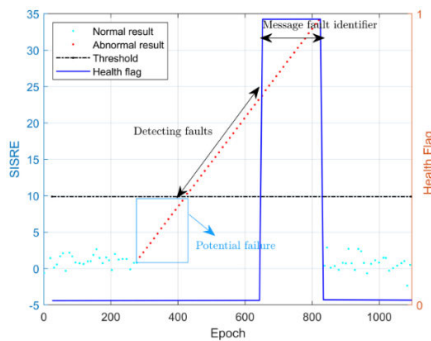


FIGURE 2. Graphical illustration of the empirical threshold method of fault detection defects.

ARDL model is a time series analysis method. In this paper, the ARDL model of SISRE calculated values under nominal conditions is built to obtain quantitative predictions using historical data of navigation and real-time orbital clock difference corrections. The measured forecasts are correlated with the previous moments in the sample space, and the measured forecasts are less affected by the fault when the fading fault occurs, and the resulting residuals are larger, thus enabling effective detection of fading SISRE faults. The ARDL model is built to extend the failure duration and thus increase the probability of failure, which is a tradeoff for potentially reducing the URA. The time error series of SISRE can be represented by the ARDL model as [28]:

$$y_t = \alpha + \sum_{i=1}^m \alpha_i Y_{t-i} + \sum_{j=1}^p \sum_{i=0}^s \beta_{ji} X_{jt-i} + \mu_t \quad (11)$$

where  $y_t$  is the predictive value of SISRE for time  $t$ ,  $\alpha_i$  is the coefficient term,  $m$  is the order of the autoregression,  $\mu_t$  is the residual error after fitting the ARDL model,  $s$  is the order of the distribution lag, and  $p$  is the order of the exogenous variables. The autoregressive coefficients  $\alpha_i$  and  $\beta_{ji}$  of the above equation are uniquely determined by the serial

autocovariance function through the Yule-Walker equation as follows.

$$\begin{bmatrix} \gamma_1 \\ \gamma_2 \\ \dots \\ \gamma_p \end{bmatrix} = \begin{bmatrix} \gamma_0 & \gamma_1 & \dots & \gamma_{p-1} \\ \gamma_1 & \gamma_0 & \dots & \gamma_{p-2} \\ \dots & \dots & \dots & \dots \\ \gamma_{p-1} & \gamma_{p-2} & \dots & \gamma_0 \end{bmatrix} \begin{bmatrix} a_1 \\ a_2 \\ \dots \\ a_p \end{bmatrix} \quad (12)$$

where  $\gamma_p$  is  $E(y_{t+p}y_t)$ ,  $p-i$  is the number of perturbation sources that affect SISRE,  $a_i$  is the coefficient term to be solved,  $\mu_t$  Gaussian white noise variance  $\sigma^2$  is:

$$\sigma^2 = \gamma_0 - (\psi_1 \gamma_1 + \psi_2 \gamma_2 + \dots + \psi_p \gamma_p) \quad (13)$$

The parameters of the ARDL model are estimated using the above method to obtain the model of each order. However, the order of the model needs to be determined in advance, and for the choice of the autoregressive order  $m$  and the lag order  $\mu_t$  can be chosen according to the information criterion.

$$\text{BIC} = -2 \ln(L) + \ln(n) * k \quad (14)$$

where  $L$  is the maximum likelihood estimate under the model,  $n$  is the number of data, and  $k$  is the number of variables in the model. In model fitting, adding parameters makes the likelihood probability increase, but introduces additional variables, so the information criterion model adds a penalty term for the number of model parameters to the objective equation as the second term. When  $n \geq 8$ ,  $\ln(n) * k \geq 2k$ , i.e., the model penalizes the model parameters more at large data volumes, leading to its preference for simple models with fewer parameters.

In the application of space signal anomaly detection, an ARDL model is first fitted by determining the model parameters using historical data. Then, the ARDL model is used to predict the current value of the space signal, which is compared to the actual value. If the prediction error exceeds a certain multiple of the standard deviation of the prediction error, an anomaly is detected. The specific steps are as follows:

1. Fit an ARDL model using historical data and determine the parameters  $m$ ,  $p$ , and  $s$  of the model using the method mentioned above.
2. Use the fitted ARDL model to predict the current value of the space signal  $Y_t$ .
3. Calculate the prediction error  $e_t = y_t - \hat{y}_t$ , where  $y_t$  is the actual SISRE value.
4. Calculate the standard deviation of the prediction error  $\sigma_y = \sqrt{\frac{1}{N-1} \sum_{t=1}^N e_t^2}$ , where  $N$  is the number of historical data.
5. If any one of the following conditions a and b is satisfied, it is judged as anomaly.

a. The comparison of the before and after ephemeris is performed. If the current prediction error of 10 consecutive ephemeris exceeds 3 times the standard deviation of the prediction error, the prediction value is taken as the threshold value until the prediction value of 10 consecutive ephemeris is less than 3 times the standard deviation of the prediction error.

b. The actual high-precision orbit and clock error exceeds the empirical threshold value, which is usually  $4.42 \times URA$ , where URA is the integrity parameter of the broadcast ephemeris.

The choice of the multiple to detect space signal anomalies depends on the specific application scenario and requirements. In general, a multiple of 2 or 3 times the standard deviation of the prediction error can be used to detect anomalies when the prediction error exceeds the multiple. This multiple can be adjusted experimentally or based on experience to achieve better results. It should be noted that setting the multiple too small will result in a high false alarm rate, while setting it too large will result in a high miss detection rate. A balance needs to be struck between false alarm and miss detection rates. For example, in the application of autonomous driving, a lower multiple may be considered to ensure safety at the expense of false alarms.

#### IV. STATISTICS AND ANALYSIS

In order to validate the performance of the combined approach based on the ARDL model and empirical threshold anomaly detection, we first analyzed the data completeness rate to exclude false anomalies caused by invalid data and spatial signals. To demonstrate the superiority of the proposed method, we compared the impact of traditional empirical thresholds and the combined approach on SISRE anomaly detection, where the traditional empirical threshold is set at  $4.42 \times URA$ . Additionally, to demonstrate the effectiveness of the combined anomaly detection method based on the autoregressive distributed lag model and empirical threshold, we conducted a statistical analysis of all SIS anomaly events identified in 2021.

##### A. DATA AVAILABILITY ANALYSIS

Long-term stable data is obtained by filtering outliers according to the pre-processing strategy. Figures 3 and 4 show the availability information for the BDS-3/BDS-2 satellite product data. When real-time satellite product data is available for this time period, which is filled with specific colors of different constellations. There are a total of 289,086 ephemeris, real-time product portfolio data points, and a total of 28,503 anomalies have been filtered out, representing about 9.86%. As can be seen from the figure, the missing data can be divided into two types: one in which almost all BDS-3/BDS-2 satellites are missing data in the same time period. Most of this is due to operational problems of NTRIP Caster, transmission network, unstable real-time data streams broadcasted by ground tracking stations, stability of BNC software, and unavailability of all satellite products in this time period may be caused by other potential factors. The other is missing data occurring from BDS-3/BDS-2 satellites in different time periods, which is mostly due to filtering out the broadcast conditions not met of the precision ephemeris.

Figure 5 shows the availability statistics of the BDS-2 and BDS-3 satellite products required for the study. The results show that the products of the GEO satellites have a higher

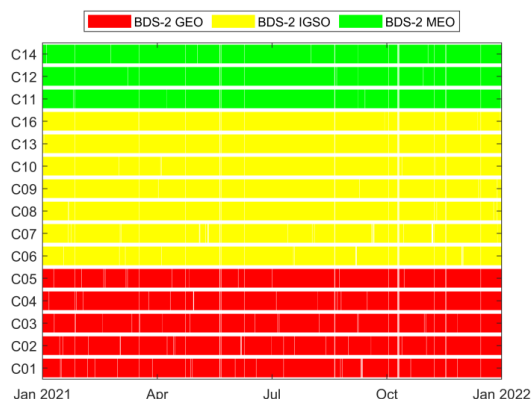


FIGURE 3. BDS-2 constellation product availability history.

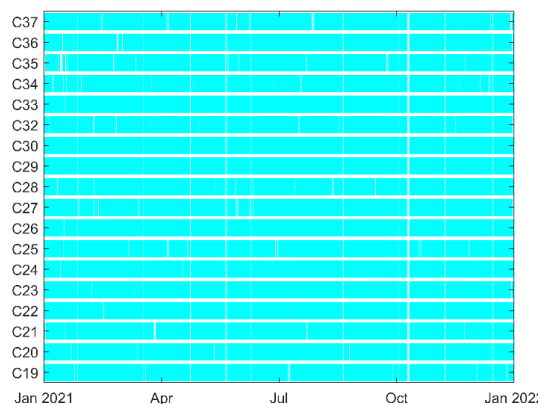


FIGURE 4. BDS-3 constellation product availability history.

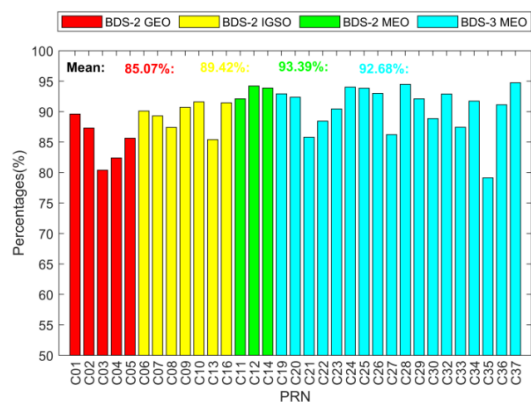


FIGURE 5. BDS-2 and BDS-3 product availability statistics.

frequency of missing data compared to the MEO and IGSO satellites. Several BDS-3 MEO satellites have more products with missing data compared to the BDS-2 MEO satellites.

As shown in Table 1, the GEO satellite availability rate was below 90% in the period. This can be attributed to the fact that GEO satellites typically have the largest number of satellite maneuvers for proper maintenance of satellites in their designed positions despite a strong 1:1 resonance between satellite revolution period and earth rotation. Among the MEO satellites, C37 has the highest availability rate of 94.7%. C35 has the lowest availability rate of 79.1%, which

TABLE 1. Satellite availability rate.

Satellite availability(%)	C01	C02	C03	C04	C05	C06	C07	C08	C09	C10	C13
Satellite availability(%)	C16	C11	C12	C14	C19	C20	C21	C22	C23	C24	C25
Satellite availability(%)	C26	C27	C28	C29	C30	C32	C33	C34	C35	C36	C37
Satellite availability(%)	89.6	87.3	80.4	82.4	85.7	90.1	89.3	87.4	90.7	91.6	85.4
Satellite availability(%)	91.4	92.1	94.2	93.8	92.9	92.4	85.8	88.4	90.4	93.6	93.1
Satellite availability(%)	86.2	94.5	92.1	88.6	94.5	92.1	87.4	91.7	79.1	91.1	94.7

is caused by a large number of data interruptions during transmission.

**B. ANALYSIS OF ANOMALY DETECTION BASED ON ARDL MODEL**

In the previous section, the integrity of the data was analyzed. After removing invalid data, this chapter analyzes the superiority of the combination method over traditional threshold methods. In order to demonstrate the application of the ARDL model in SIS anomaly detection, the detection results of two SISRE normal and abnormal are compared in this paper. As shown in Figures 5 and 6, the black dashed line in the figure indicates the threshold value for anomaly detection using the empirical threshold method of 10 m, the red line indicates the threshold value of anomaly detection using the combined method based on the ARDL model and empirical threshold, and the blue dots indicate the trend of SISRE.



FIGURE 6. Performance of two detection methods in normal SIS.

Figure 6 shows the normal results of SISRE for the BJFS gauging station at DOY 270 C25 of annual cumulative days in 2021. As can be seen from Figure 4, both fault detection methods did not reach the threshold under the no-fault condition, and the detection results were comparable, with no false alarm cases.

Figure 7 shows the anomaly results of the SISRE at the BJFS station for the annual cumulative day 289 days C30 in 2021. The detection results for the whole day are not shown in the figure due to the lack of real-time orbit and clock difference correction data for the part of the day. Many studies have shown that when spatial signals experience anomalies, they are often accompanied by regular changes. The clock error typically exhibits a linear slope, while the orbit error typically exhibits a sinusoidal variation. There is a potential for failure to occur before the trend error reaches the threshold [29].

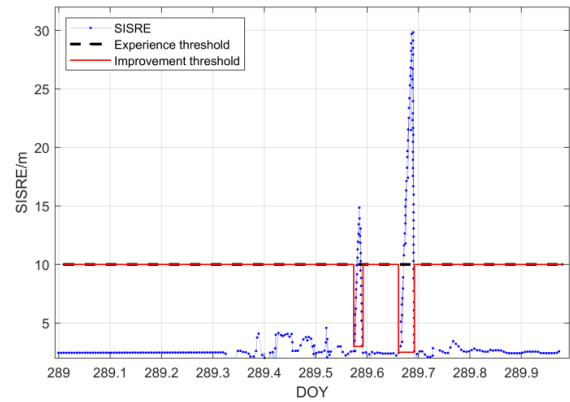


FIGURE 7. Difference of two detection methods in SIS anomaly.

The two consecutive anomalies in a short period of time are mainly due to the increase of forecast clock errors, which cause the SISRE to accumulate and exceed the threshold value after a period of time. The empirical threshold method detected the anomalies that exceeded the threshold part, but did not detect the anomalies that did not exceed the threshold part of the trend, leading to an increase in the false alarm rate of the satellite. The combination method based on autoregressive distributed lag model and empirical threshold performs well in both anomaly results in the figure, and accurately identifies the anomaly onset when an anomaly trend occurs, this method increases the satellite failure probability, but is necessary for life safety applications.

**C. ANOMALY STATISTICS**

Figure 8 shows all SIS anomalous events identified in 2021 based on the ARDL model combined with the empirical threshold anomaly detection method. The green line represents the normal SIS performance, the red star symbols represent the SIS anomalies caused by clock anomalies, and the blue triangle symbols represent the SIS anomalies due to orbital anomalies. The results show that there are significantly more SIS anomalies caused by clock anomalies than those caused by orbits. The reason for this is that since the orbital anomalies are specific to sinusoidally trending anomalies, it is not effective in detecting the anomalies triggered by them using the autoregressive distributed lag model, thus not detecting all the anomalies that do not reach the empirical threshold. In addition, most BDS satellites have SIS anomalies, and GEO and IGSO have a higher probability of SIS anomalies than MEO satellites, but because there are more BDS MEO satellites, the overall reflection is that MEO anomalies occur the most often. The range of

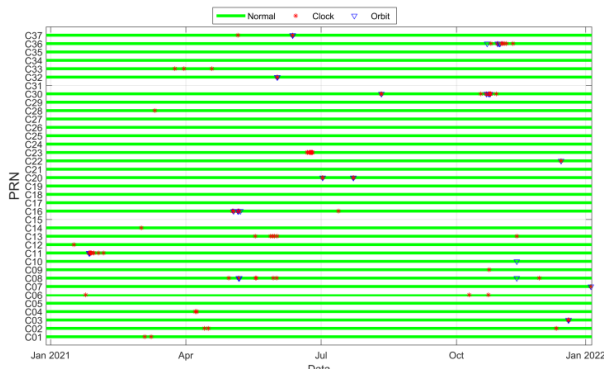
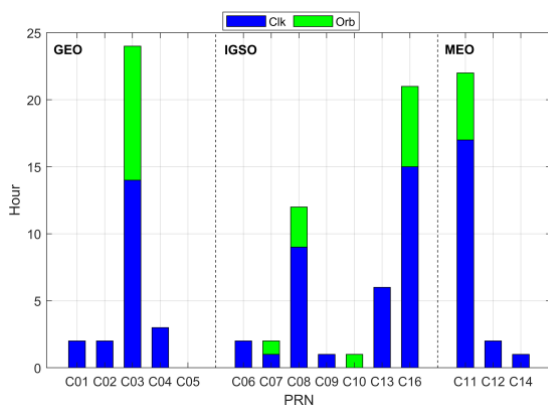
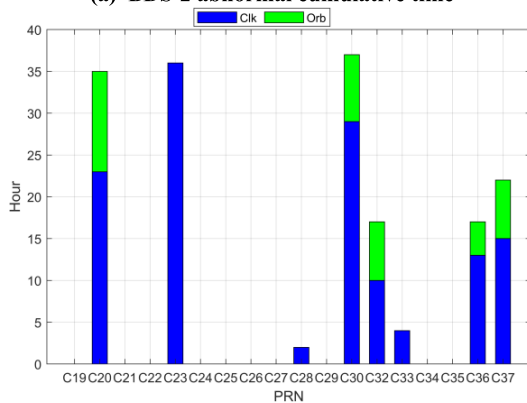


FIGURE 8. SIS anomaly distribution over time.



(a) BDS-2 abnormal cumulative time



(b) BDS-3 abnormal cumulative time

FIGURE 9. Total accumulation of anomalies for BDS satellites in 2021.

SIS anomalies for BDS varies from a few meters to several hundred kilometers. Concurrent SIS anomalies of single and multiple satellites in different ranges also occurred during the system operation.

The total accumulation of satellite anomalies for the 2021 BDS is shown in Figure 9. The results demonstrate that the cumulative anomaly duration of satellite C23 exceeds 35 h, which is mainly caused by clock errors. Satellites C01, C02, C06, and C11 have the same anomaly duration and are anomalous for the same period. During the analysis period, there are some satellites with no anomalies detected, which may also be due to the satellite anomalies not reaching the empirical threshold and not trending. Satellites with

longer anomaly durations were often accompanied by orbital anomalies (except for C23, where only clock anomalies occurred). The highest frequency of clock anomalies and fewer orbital anomalies among the anomalous events may also be attributed to the better detection capability of the method for clock anomalies.

## V. CONCLUSION

Signal-in-space anomalies are one of the main sources of risk for users in PNT services. However, the traditional SIS anomaly monitoring method cannot be applied to BDS due to the high frequency of spatial signal anomalies triggered by clock anomalies in BDS. The traditional empirical threshold method is difficult to identify the start and end times of trending faults, which further increases the false alarm rate of satellites. In this study, a high-precision spatial signal anomaly detection method based on the combination of ARDL model and empirical threshold is proposed to detect BDS high-precision spatial signal anomaly. The following are the specific research results.

1) To exclude spurious SIS anomalies, the data quality of BDS-2 and BDS-3 during the evaluation period was analyzed. The results show that BDS-2 MEO has a high missing data rate of 14.93% relative to other orbit types. Except for C35, the data availability of BDS-3 MEO satellites exceeded 85% with an average value of 92.68%. The average real-time data availability of BDS-2 MEO and BDS-2 IGSO satellites are 93.39% and 89.42%, respectively.

2) Due to the fact that many occurrences of anomalous signals in the BeiDou satellite system are due to clock anomalies, the traditional SIS anomaly monitoring methods have poor performance when applied to monitoring the BeiDou system. Based on this problem, we propose a high-precision space signal anomaly detection method for detecting BDS high-precision space signal anomalies, which combines autoregressive distribution lag models with empirical threshold values. Compared with the traditional empirical threshold method, our method can accurately identify the start and end times of anomalies. By using data from the past year and applying our proposed method, we have identified a total of 271 single-satellite SIS anomaly events and 2 multi-satellite concurrent SIS anomaly events. The detected anomalies are mainly caused by clock errors, orbit errors, and their combined defects. Among the identified anomalies, clock errors account for approximately 73.43%, orbit errors account for approximately 20.66%, and the combination of the two accounts for approximately 5.91%.

## VI. CONFLICTS OF INTEREST

There is no conflict of interest regarding the publication of this article.

## REFERENCES

- [1] O. Montenbruck, P. Steigenberger, and A. Hauschild, "Multi-GNSS signal-in-space range error assessment—Methodology and results," *Adv. Space Res.*, vol. 61, no. 12, pp. 3020–3038, Jun. 2018.



- [2] S. Gu, R. Guo, X. Gong, S. Zhang, Y. Lou, and Z. Li, "Real-time precise point positioning based on BDS-3 global short message communication," *GPS Solutions*, vol. 26, no. 4, pp. 1–14, Oct. 2022.
- [3] K. Kazmierski, R. Zajdel, and K. Sosnica, "Evolution of orbit and clock quality for real-time multi-GNSS solutions," *GPS Solutions*, vol. 24, no. 4, pp. 2447–2463, Oct. 2020.
- [4] S. Perea, M. Meurer, M. Rippl, B. Belabbas, and M. Joerger, "URA/SISA analysis for GPS and Galileo to support ARAIM," *Navigation*, vol. 64, no. 2, pp. 237–254, Jun. 2017.
- [5] B. Xue, H. Wang, and Y. Yuan, "Performance of BeiDou-3 signal-in-space ranging errors: Accuracy and distribution," *GPS Solutions*, vol. 25, no. 1, p. 23, Jan. 2021.
- [6] H. Jiang, H. Wang, Z. Wang, and Y. Yuan, "Real-time monitoring for BDS signal-in-space anomalies using ground observation data," *Sensors*, vol. 18, no. 6, p. 1816, Jun. 2018.
- [7] L. Heng, G. X. Gao, T. Walter, and P. Enge, "GPS signal-in-space integrity performance evolution in the last decade," *IEEE Trans. Aerosp. Electron. Syst.*, vol. 48, no. 4, pp. 2932–2946, Oct. 2012.
- [8] Y. Wu, J. Ren, and W. Liu, "Preliminary analyses of BeiDou signal-in-space anomaly since 2013," *Int. Arch. Photogramm., Remote Sens. Spatial Inf. Sci.*, vol. 41, pp. 517–523, Jan. 2019.
- [9] K. Gunning, T. Walter, and P. Enge, "Characterization of GLONASS broadcast clock and ephemeris: Nominal performance and fault trends for ARAIM," in *Proc. Int. Tech. Meeting Inst. Navigat.*, Mar. 2017, pp. 170–183.
- [10] L. Fan, R. Tu, R. Zhang, Z. Zheng, J. Liu, J. Hong, and X. Lu, "Real-time BDS signal-in-space anomaly detection method considering receiver anomalies," *IET Radar, Sonar Navigat.*, vol. 13, no. 12, pp. 2220–2229, Dec. 2019.
- [11] L. Fan, R. Tu, R. Zhang, Z. Zheng, X. Lu, J. Liu, X. Huang, and J. Hong, "An improved method for detecting BeiDou signal-in-space anomalies from precise ephemerides," *Acta Geodaetica et Geophysica*, vol. 54, no. 4, pp. 567–581, Dec. 2019.
- [12] C. Ouyang, J. Shi, Y. Shen, and L. Li, "Six-year BDS-2 broadcast navigation message analysis from 2013 to 2018: Availability, anomaly, and SIS UREs assessment," *Sensors*, vol. 19, no. 12, p. 2767, Jun. 2019.
- [13] L. Fan, R. Tu, R. Zhang, J. Han, P. Zhang, J. Hong, and X. Lu, "Detection and analysis of Galileo signal in space anomalies from 2017 to 2018," *IET Radar, Sonar Navigat.*, vol. 14, no. 11, pp. 1690–1696, Nov. 2020.
- [14] G. Huang, Z. Qin, Q. Zhang, L. Wang, X. Yan, and X. Wang, "An optimized method to detect BDS satellites' orbit maneuvering and anomalies in real-time," *Sensors*, vol. 18, no. 3, p. 726, Feb. 2018.
- [15] F. Li, R. Tu, J. Hong, S. Zhang, P. Zhang, and X. Lu, "Combined positioning algorithm based on BeiDou navigation satellite system and raw 5G observations," *Measurement*, vol. 190, Feb. 2022, Art. no. 110763.
- [16] Y. Zhou, Y. Wang, W. Huang, and L. Sun, "Statistical characterization of GNSS signal-in-space ranging errors for the user within and beyond space service volume," *IEEE Access*, vol. 7, pp. 168116–168125, 2019.
- [17] S. Perea, M. Meurer, and B. Pervan, "Impact of sample correlation on SISRE overbound for ARAIM," *Navigation*, vol. 67, no. 1, pp. 197–212, Mar. 2020.
- [18] R. Tu, R. Zhang, L. Fan, J. Han, P. Zhang, X. Wang, J. Hong, J. Liu, and X. Lu, "Real-time monitoring of the dynamic variation of satellite orbital maneuvers based on BDS observations," *Measurement*, vol. 168, Jan. 2021, Art. no. 108331.
- [19] B. Li, H. Ge, Y. Bu, Y. Zheng, and L. Yuan, "Comprehensive assessment of real-time precise products from IGS analysis centers," *Satell. Navigat.*, vol. 3, no. 1, p. 12, Dec. 2022.
- [20] T. Geng, Z. Li, X. Xie, W. Liu, Y. Li, and Q. Zhao, "Real-time ocean precise point positioning with BDS-3 service signal PPP-B2b," *Measurement*, vol. 203, Nov. 2022, Art. no. 111911.
- [21] Z. Ren, H. Gong, J. Peng, C. Tang, X. Huang, and G. Sun, "Performance assessment of real-time precise point positioning using BDS PPP-B2b service signal," *Adv. Space Res.*, vol. 68, no. 8, pp. 3242–3254, Oct. 2021.
- [22] F. Li, R. Tu, J. Hong, S. Zhang, M. Liu, and X. Lu, "Performance analysis of BDS-5G combined precise point positioning," *Remote Sens.*, vol. 14, no. 13, p. 3006, Jun. 2022.
- [23] O. Montenbruck, P. Steigenberger, and M. Aicher, "A long-term broadcast ephemeris model for extended operation of GNSS satellites," *Navigation*, vol. 68, no. 1, pp. 199–215, Mar. 2021.
- [24] G. Chen, R. Zhou, Z. Hu, Y. Lv, N. Wei, and Q. Zhao, "Statistical characterization of the signal-in-space errors of the BDS: A comparison between BDS-2 and BDS-3," *GPS Solutions*, vol. 25, no. 3, Jul. 2021.
- [25] K. Gunning, T. Walter, and P. Enge, "Multi-GNSS constellation anomaly detection and performance monitoring," in *Proc. 30th Int. Tech. Meeting Satell. Division Inst. Navigat.*, Portland, Oregon, Nov. 2017, pp. 1051–1062.
- [26] Y. Yang, Y. Xu, J. Li, and C. Yang, "Progress and performance evaluation of BeiDou global navigation satellite system: Data analysis based on BDS-3 demonstration system," *Sci. China Earth Sci.*, vol. 61, no. 5, pp. 614–624, May 2018.
- [27] G. Xiao, G. Liu, J. Ou, C. Zhou, Z. He, R. Chen, A. Guo, and Z. Yang, "Real-time carrier observation quality control algorithm for precision orbit determination of LEO satellites," *GPS Solutions*, vol. 26, no. 4, pp. 1–15, Oct. 2022.
- [28] R. K. Nayak, "Performance of Odisha state co-operative bank: An ARDL approach," *Arthaniti, J. Econ. Theory Pract.*, vol. 21, no. 1, pp. 7–26, Jun. 2022.
- [29] T. Walter, J. Blanch, K. Gunning, M. Joerger, and B. Pervan, "Determination of fault probabilities for ARAIM," *IEEE Trans. Aerosp. Electron. Syst.*, vol. 55, no. 6, pp. 3505–3516, Dec. 2019.



**LIANG LIU** was born in Heilongjiang, China, in May 1989. He received the M.Eng. degree in electronic and communication engineering from the Harbin Institute of Technology, in 2014.

In 2014, he joined the 54th Research Institute of China Electronics Technology Group Corporation and carried out research on signal monitoring and performance evaluation technology with the State Key Laboratory of Satellite Navigation System and Equipment Technology.



**HUICHAO LIU** was born in Heilongjiang, China, in 1997. He received the B.S.E. degree in electrical engineering and automation from Heilongjiang Bayi Agricultural University, Heilongjiang, in 2020. He is currently pursuing the M.Eng. degree in electronic information with Shenyang Aerospace University, Shenyang, China.

His current research interests include satellite navigation and positioning technology.



**ERSHEN WANG** was born in Liaoning, China, in 1980. He received the Ph.D. degree in communication and information systems from Dalian Maritime University, China, in 2009.

From January 2014 to December 2016, he was a Postdoctoral Researcher with Beihang University, China. He is currently a Professor with the School of Electronic and Information Engineering, Shenyang Aerospace University, Shenyang, China. He is also a member of the Liaoning General Aviation Academy, Shenyang. He is the lead of the Key Laboratory of Navigation and Surveillance Technology. He has published more than 80 articles in peer-reviewed journals and proceedings and 20 patents/software copyrights. His current research interests include BeiDou navigation satellite systems (BDSs)/global navigation satellite systems (GNSSs) positioning theory and signal processing, integrity monitoring, integrated navigation, target tracking, artificial intelligence, and applications to unmanned systems.



**TENGLI YU** was born in Hebei, China, in 1997. She received the B.S.E. degree in geomatics engineering from Shijiazhuang Tiedao University, Shijiazhuang, China, in 2019, and the M.Eng. degree in geomatics engineering from Tianjin Chengjian University, Tianjin, China, in 2022. She is currently pursuing the Ph.D. degree with Shenyang Aerospace University, Shenyang, China.

Her current research interests include the global navigation satellite systems (GNSSs) technology and resilient PNT technology for aircraft.



**TENG LONG** was born in Liaoning, China, in March 1993. He received the D.Eng. degree in aeronautical and astronautical science and technology from the Harbin Institute of Technology, in 2022.

In 2022, he joined the 54th Research Institute of China Electronics Technology Group Corporation and carried out research on satellite navigation baseband signal processing with the State Key Laboratory of Satellite Navigation System and Equipment Technology.



**SHIYU JIA** was born in Hebei, China, in May 1991. He received the M.Eng. degree in electronic information engineering from Beihang University, in 2017.

In 2017, he joined the 54th Research Institute of China Electronics Technology Group Corporation and carried out research on signal monitoring and performance evaluation technology with the State Key Laboratory of Satellite Navigation System and Equipment Technology.



**XINHUI SUN** was born in Liaoning, China, in 2000. She received the B.S.E. degree in communication engineering from Shenyang Aerospace University, Shenyang, China, in 2021, where she is currently pursuing the M.Eng. degree in electronic information.

Her current research interests include satellite navigation and positioning technology.

...